Available online at www.sciencedirect.com

ScienceDirect

Procedia Structural Integrity 24 (2019) 53–65

Structural Integrity Procedia

www.elsevier.com/locate/procedia

AIAS 2019 International Conference on Stress Analysis

An Enhanced Material Model for the Simulation of High-Velocity Impact on Fiber-Reinforced Composites

Riccardo Scazzosi[a*], Andrea Manes[a], Marco Giglio[a]

[a]*Politecnico di Milano, Dipartimento di Meccanica, Via La Masa 1, Milan 20156, Italy*

Abstract

Composite MSC (MAT_161 and MAT_162) is an enhanced material model for fiber-reinforced composites implemented in the software LS-DYNA which considers different failure modes in tension, compression and shear, with a progressive failure model. It allows to model delamination without the necessity of physical interface between the layers. Furthermore, it considers the effect of strain rate on the strength and moduli properties of the materials by means of a logarithmic function. Several studies can be found in the literature where the material model Composite MSC is implemented for modeling glass fiber-reinforced composites while it is difficult to find studies related to aramid fiber-reinforced composites. Aramid fibers are used in the manufacturing of ballistic shields since they are characterized by high tensile strength and resistance to impact damage. In this study the predictive accuracy of the material model Composite MSC (in particular MAT_162) for aramid fiber-reinforced composites is assessed simulating the high-velocity impact of a .357 Magnum projectile considering different impact velocities and therefore different scenarios from the arrest of the projectile to the full penetration of the target. MAT_162 is compared with MAT_058 which is a simpler material model which needs less input materials parameters and is therefore easier to be implemented. Furthermore, a parametric study on input parameters which are considered to be relevant is performed.

Keywords: high-velocity impact; ballistic; fiber-reinforced composite; aramid fiber; Kevlar; numerical model.

* Corresponding author. Tel.: +39 02 2399 8630 ; fax: +39 02 2399 8263.
E-mail address: riccardo.scazzosi@polimi.it

10.1016/j.prostr.2020.02.005

1. Introduction

Ballistic shields are used whenever it is necessary to protect valuables or lives from an external threat. Fiber-reinforced composites are a preferred choice for the manufacturing of ballistic shields due to their favorable combination of high strength and low weight, especially for the protection of vehicles, where a lower weight leads to lower fuel consumption or increased payload. Aramid fibers are used when high tensile strength and resistance to impact damage are important (Mallick 2007), this is the reason why they are extensively used in the manufacturing of ballistic shields. Many works can be found in the literature in which numerical models for the simulation of high-velocity impact on aramid fiber-reinforced composites using a macro-scale approach are developed (Tham, Tan, and Lee 2008; Gower, Cronin, and Plumtree 2008; Manes, Bresciani, and Giglio 2014; Y. Q. Li, Li, and Gao 2015; Bresciani et al. 2016; Scazzosi et al. 2018; Nunes et al. 2019; Berk, Karakuzu, and Toksoy 2017; Kumar et al. 2010; Nayak, Banerjee, and Panda 2017). In this approach the material is modeled as an equivalent homogeneous medium with no distinction between its constituents. The mechanical behaviour of the material is modeled using orthotropic elasticity and different failure criteria which considers the different failure modes of composites.

Composite MSC (MAT_161 and MAT_162) is an enhanced material model for fiber-reinforced composites implemented in the software LS-DYNA which considers different failure modes in tension, compression and shear with a progressive failure model. It allows the modelling of delamination without the necessity of a physical interface between the layers. Furthermore, it considers the effect of strain rate on the strength and moduli properties of the materials by means of a logarithmic function (Material Science Corporation (MSC) & University of Delaware Center for Composite Materials (UD-CCM) 2017). However 34 input parameters are necessary for its implementation (Gama and Gillespie 2011). Several studies can be found in the literature where the material model Composite MSC is implemented for modeling glass fiber-reinforced composites (Gama and Gillespie 2011; Xiao, Gama, and Gillespie 2007; Deka, Bartus, and Vaidya 2008; Jordan, Naito, and Haque 2014; J. Li et al. 2019), while it is difficult to find studies related to aramid fiber-reinforced composites. In (Y. Q. Li, Li, and Gao 2015; X. G. Li, Gao, and Kleiven 2016) the material model Composite MSC is used for the simulation of high-velocity impact on a combat helmet, which is manufactured from aramid fiber-reinforced composites, but this studies focus only on the case of a projectile arrest without partial or full penetration of the target.

In this study the predictive accuracy of the material model Composite MSC (in particular MAT_162) for aramid fiber-reinforced composites is assessed simulating the high-velocity impact of a .357 Magnum projectile considering different impact velocities and therefore different scenarios from the arrest of the projectile to the full penetration of the target. MAT_162 is compared with MAT_058 which is a simpler material model which needs less input materials parameters and is therefore easier to be implemented. The models predictions are compared with experimental result already obtained by the authors in (Scazzosi, Manes, and Giglio 2019), where an innovative analytical model for high-velocity impact on fiber-reinforced composites was developed. Furthermore, a parametric study on input parameters which are considered to be relevant is performed. In section 2 the numerical models are described while the results of the simulation are discussed in section 3. Finally, conclusions are drawn in section 4.

2. Numerical Model

Two numerical models were developed to simulate high-velocity impact on fiber reinforced composites using the software LS-DYNA mpp d R11.0.0. In particular, the numerical models were aimed at reproducing experimental tests already performed by the authors for the validation of an innovative analytical model of high-velocity impact on fiber-reinforced composites (Scazzosi, Manes, and Giglio 2019). In these experimental tests high-velocity impacts of a .357 Magnum projectile against composite panels were performed. Composite panels consisted of 14 layers of plain wave Kevlar 29 fabric embedded in an epoxy matrix. This material has already been characterized by the authors by means of tensile tests (Scazzosi et al. 2018): the elastic modulus was 10.06±0.65 GPa (calculated in the strain range between 1.8 and 2.2%) and the tensile strength was 405.24±18.03 MPa. The two numerical models differ in the material model used for the composite panel: Laminated Composite Fabric (MAT_058) and Composite MSC (MAT_162). These two material models require different element types, as explained in sections 2.1 and 2.2.

The two numerical models are shown in Figure 1. They are three-dimensional and are developed exploiting the double symmetry of the problem, therefore only one quarter of the projectile and the target are modelled. Symmetry boundary conditions are then applied to the faces of the projectile and the target which lie on a symmetry plane. This is a common procedure followed for this type of simulations in order to decrease the computational cost (Scazzosi et al. 2018; Manes, Bresciani, and Giglio 2014; Bresciani et al. 2016; Gower, Cronin, and Plumtree 2008; Berk, Karakuzu, and Toksoy 2017; Nunes et al. 2019). The projectile is made of two parts, the lead core and the brass jacket, which are modeled using constant-stress solid element with complete integration. The material model for these two parts is the Modified Johnson-Cook with Cockcroft-Latham failure criterion (MAT_107) whose input parameter are reported in Table 1. E and ν are respectively the elastic modulus and the Poisson's ratio, A, B and n are the Johnson-Cook strain hardening parameters, C is the strain rate sensitivity parameter and $\dot{\epsilon}_0$ the reference strain rate, m is the thermal softening parameters and T_m is the melting temperature and W_{cr} is the Cockcroft-Latham parameter. The parameter C was obtained by fitting the Modified Johnson-Cook equation for strain rate sensitivity with the Johnson-Cook equation used in the original reference ((Gilioli et al. 2015) and (Zukas 1990) for respectively lead and brass).

Table 1. MAT_107 input parameters for the lead core and brass jacket.

Material	Lead	Brass
E (MPa)	16000 (Gilioli et al. 2015)	115000 (Børvik, Dey, and Clausen 2009)
ν	0.42 (Gilioli et al. 2015)	0.31 (Børvik, Dey, and Clausen 2009)
A (MPa)	0 (Gilioli et al. 2015)	111.69 (Zukas 1990)
B	55.552 (Gilioli et al. 2015)	504.69 (Zukas 1990)
n	0.0987 (Gilioli et al. 2015)	0.42 (Zukas 1990)
$\dot{\epsilon}_0$ (s^{-1})	72.108 (Gilioli et al. 2015)	1 (Zukas 1990)
C	0.126	0.0085
T_m (K)	525 (Gilioli et al. 2015)	1189 (Børvik, Dey, and Clausen 2009)
m	1 (Gilioli et al. 2015)	1.68 (Zukas 1990)
W_{cr} (MPa)	175 (Børvik, Dey, and Clausen 2009)	914 (Børvik, Dey, and Clausen 2009)

Fig. 1. Numerical model for (a) MAT_058 and (b) MAT_162.

The target is a composite panel which is modelled as a quarter of 80x80 mm and a thickness of 6.5 mm (Scazzosi, Manes, and Giglio 2019). More details are given in section 2.1 and 2.2 since the mesh of the panels depends on the material model used. All degrees of freedom are fixed on the outer edges to model the effect of the fixing frame.

1.1. MAT_058: Laminated Composite Fabrics

The material model Laminated Composite Fabrics (MAT_058) is based on Matzenmiller, Lubliner and Taylor constitutive model for anisotropic damage in fiber-reinforced composites (Matzenmiller, Lubliner, and Taylor 1995). This material model is limited to unidirectional fiber-reinforced composites but two additional material models were implemented in MAT_058 which follow the damage approach developed in (Matzenmiller, Lubliner, and Taylor 1995) and are suitable for woven fabrics composites (Schweizerhof et al. 1998). Here the material model with a smooth failure surface denoted as material 58b (chosen by selecting FS = 1 in the material card) is described since it is the one adopted in this study. The failure criterion is the same in the 11- and 22-direction as defined in Eq. (1) and Eq. (2)

$$f_{11} = \frac{\sigma_{11}^2}{\left(1-\omega_{11c,t}\right)^2 X_{c,t}^2} + \frac{\tau^2}{(1-\omega_{12})^2 S_c^2} - r_{||c,t} = 0 \tag{1}$$

$$f_{22} = \frac{\sigma_{22}^2}{\left(1-\omega_{22c,t}\right)^2 Y_{c,t}^2} + \frac{\tau^2}{(1-\omega_{12})^2 S_c^2} - r_{||c,t} = 0 \tag{2}$$

where $X_{c,t}$, $Y_{c,t}$ and S_c are the material strengths, as described in Table 2, ω is a damage parameter which is different in tension and in compression for the 11- and 22-direction, in order to account one-sidedness which is typical in many materials, while it does not depend on the shear direction (12-direction). For a complete description of the damage evolution the reader is referred to (Schweizerhof et al. 1998). The damage evolution is modified such that stress does not fall below a threshold value. This threshold value is defined by the parameters called SLIMxx which is the ratio between the strength and the threshold value (σ_{min}) as defined in Eq. (3) (Livemore Software Technology Corporation (LSTC) 2017)

$$\sigma_{min} = SLIM_{xx} \cdot strength \tag{3}$$

The user can thus define different threshold values for the 11- and 22-direction in tension and compression (respectively SLIMT1, SLIMC1, SLIMT2 and SLIMC2) and in the 12-direction (SLIMS). A small value for tensile failure (SLIMT1 and SLIMT2) is usually preferred, between 0.05 and 0.1, while a value of 1 is usually preferred in compression (SLIMC1 and SLIMC2) and shear (SLIMS) (Livemore Software Technology Corporation (LSTC) 2017).

It is possible to define the values of the material strength as a function of the strain rate by means of tabular data. This option is preferred in this study since MAT_162 also includes the effects of strain rates and it is intended to develop the two numerical modes as close as possible for a more meaningful comparison. Therefore, the strength in tension and compression in the 11- and 22-directon (respectively X_t, Y_t, X_c and Y_c) are defined as a function of the strain rate following Eq. (4) (which is the same function used in MAT_162)

$$\sigma = \sigma_0 \left[1 + C_{rate1} ln\left(\frac{\dot{\epsilon}}{\dot{\epsilon}_0}\right)\right] \tag{4}$$

where σ is the strength at the strain rate $\dot{\epsilon}$, σ_0 is the static strength, $C_{rate1} = 0.0257$ (Y. Q. Li, Li, and Gao 2015) and $\dot{\epsilon}_0 = 1\ s^{-1}$ to be consistent with MAT_162. In both the 11- and 22- direction, the static strength in tension is 405 MPa (Scazzosi et al. 2018) while the compressive strength is 185 MPa (Bresciani et al. 2016).

The curves obtained by means of Eq. (4) and given as an input to the software are shown in Figure 2.

Table 2. MAT_058 input parameters for Kevlar29/Epoxy.

Symbol	Property	Value
ρ	Density	1025 kg/m^3 (Scazzosi et al. 2018)
E_a	Elastic modulus 1	10.06 GPa (Scazzosi et al. 2018)
E_b	Elastic modulus 2	10.06 GPa (Scazzosi et al. 2018)
E_c	Elastic modulus 3	6 GPa (Bresciani et al. 2016)
ν_{ba}	Poisson's ratio 21	0.25 (Bresciani et al. 2016)
ν_{ca}	Poisson's ratio 31	0.33 (Bresciani et al. 2016)
ν_{cb}	Poisson's ratio 32	0.33 (Bresciani et al. 2016)
G_{ab}	Shear modulus 12	0.77 GPa (Bresciani et al. 2016)
G_{bc}	Shear modulus 23	5.43 GPa (Bresciani et al. 2016)
G_{ca}	Shear modulus 31	5.43 GPa (Bresciani et al. 2016)
X_t	Tensile strength 1	Defined as a function of the strain rate (see Figure 2(a))
Y_t	Tensile strength 2	Defined as a function of the strain rate (see Figure 2(a))
X_c	Compressive strength 1	Defined as a function of the strain rate (see Figure 2(b))
Y_c	Compressive strength 2	Defined as a function of the strain rate (see Figure 2(b))
S_c	Shear strength 12 plane	77 MPa (Bresciani et al. 2016)
SLIMT1	Factor to determine the minimum stress limit (tension 1)	0.1
SLIMT2	Factor to determine the minimum stress limit (tension 2)	0.1
SLIMC1	Factor to determine the minimum stress limit (compression 1)	1
SLIMC2	Factor to determine minimum stress limit (compression 2)	1
SLIMS	Factor to determine minimum stress limit (shear)	1
ERODS	Maximum effective strain for element erosion	1

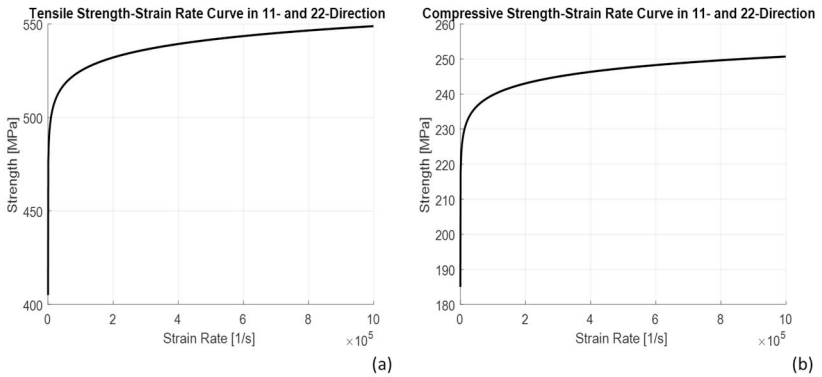

Fig. 2. Strength-strain rate curve in 11- and 22- direction in (a) tension and (b) compression.

ERODS is the maximum effective strain for element erosion which is necessary to remove overstrained elements from the model. This value must be chosen so that it does not affect the failure criterion and that the model is not polluted by overstrained elements (Barauskas and Abraitiene 2013).

The material input parameters for Kevlar29/Epoxy are reported in Table 2.

MAT058 is restricted to shell and thick shell elements only, therefore each layer of the panel is modeled as a separate part, with only one thick shell element trough the thickness (see Figure 1(a)). The dimensions of the elements are 1x1x0.445 mm where 0.445 mm is the average thickness of the layers. The interaction between the layers is modelled by means of AUTOMATIC_SURFACE_TO_SURFACE_TIEBREAK contact algorithm: the nodes which lie on the faces at the interface between two adjacent layers are tied until the interface failure criterion, given by Eq. (5), is satisfied

$$\left(\frac{\sigma_n}{S_n}\right)^2 + \left(\frac{\tau}{S_s}\right)^2 - 1 \geq 0 \tag{5}$$

where S_n is the interfacial normal stress threshold and S_s is the interfacial shear stress threshold which are considered to be equal to respectively 34.5 MPa and 9 MPa (Bresciani et al. 2016).

1.2. MAT_162: Composite MSC

The material model Composite MSC (MAT_161 and MAT_162) may be used to model progressive failure of either unidirectional or woven fabrics composites. In particular MAT_162 is used in this study, which is a generalization of MAT_161, and adopts the damage mechanic approach of Matzenmiller, Lubliner and Taylor to characterize the softening behaviour after damage initiation (Matzenmiller, Lubliner, and Taylor 1995). Here the material model for woven fabrics is described (chosen by selecting AMODEL = 2 in the material card) since it is the one adopted in this study. Seven failure criteria are adopted; the tension-shear fiber mode failures are defined in Eq. (6) and Eq. (7)

$$f_7 - \mathrm{r}_7^2 = \left(\frac{E_a\langle\epsilon_1\rangle}{S_{aT}}\right)^2 + \left(\frac{G_{ca}\epsilon_{31}}{S_{aFS}}\right)^2 - r_7^2 \tag{6}$$

$$f_8 - \mathrm{r}_8^2 = \left(\frac{E_b\langle\epsilon_2\rangle}{S_{bT}}\right)^2 + \left(\frac{G_{bc}\epsilon_{23}}{S_{bFS}}\right)^2 - r_7^2 \tag{7}$$

where E_a, E_b, G_{ca}, G_{bc}, S_{aT}, S_{bT} and S_{FS} are the material input parameters as defined in Table 3, $S_{aFS} = S_{FS}$ and $S_{bFS} = S_{FS}xS_{bT}/S_{aT}$.

The compression fiber mode failures are defined in Eq. (8) and Eq. (9)

$$f_9 - \mathrm{r}_9^2 = \left[\frac{E_a\left(-\epsilon_1 - \langle\epsilon_3\rangle\frac{E_c}{E_a}\right)}{S_{aC}}\right]^2 - r_9^2 \tag{8}$$

$$f_{10} - \mathrm{r}_{10}^2 = \left[\frac{E_b\left(-\epsilon_2 - \langle\epsilon_3\rangle\frac{E_c}{E_b}\right)}{S_{bC}}\right]^2 - r_{10}^2 \tag{9}$$

where E_c, S_{aC} and S_{bC} are the material input parameters as defined in Table 3.

The crush mode failure is defined in Eq. (10)

$$f_{11} - \mathrm{r}_{11}^2 = \left(\frac{E_c\langle -\epsilon_3\rangle}{S_{FC}}\right)^2 - r_{11}^2 \tag{10}$$

where S_{FC} is a material input parameter as defined in Table 3.
The in-plane matrix mode failure is defined in Eq. (11)

$$f_{12} - \mathrm{r}_{12}^2 = \left(\frac{G_{ab}\langle \epsilon_{12}\rangle}{S_{ab}}\right)^2 - r_{12}^2 \tag{11}$$

where G_{ab} and S_{ab} are the material input parameters as defined in Table 3.
The parallel matrix mode failure (delamination) is defined in Eq. (12)

$$f_{13} - \mathrm{r}_{13}^2 = S^2\left\{\left(\frac{E_c\langle \epsilon_3\rangle}{S_{cT}}\right)^2 + \left(\frac{G_{bc}\epsilon_{23}}{S_{bc0} + S_{SRC}}\right)^2 + \left(\frac{G_{ca}\epsilon_{31}}{S_{ca0} + S_{SRC}}\right)^2\right\} - r_{13}^2 \tag{12}$$

where S_{cT}, S_{bc0} and S_{ca0} are the material input parameters as defined in Table 3. S_{SRC} is defined as

$$S_{SRC} = E_c \tan\phi \,\langle -\epsilon_3\rangle \tag{13}$$

where ϕ is the Coulomb's friction angle.
S is a scale factor introduced to provide a better correlation of the delamination area with experiments.
For a complete description of the damage evolution the reader is referred to (Material Science Corporation (MSC) & University of Delaware Center for Composite Materials (UD-CCM) 2017).
MAT_162 also accounts for the effect of the strain rate by a logarithmic function on the strength and moduli properties, as defined respectively in Eq. (14) and Eq. (15)

$$\{S_{RT}\} = \{S_0\}\left[1 + C_{rate1}\ln\left(\left\{\frac{\dot{\bar{\epsilon}}}{\dot{\bar{\epsilon}}_0}\right\}\right)\right] \tag{14}$$

where C_{rate1} is a material input parameter as defined in Table 3, $\{S\} = \{S_{aT}\ S_{aC}\ S_{bT}\ S_{bC}\ S_{FC}\ S_{FS}\}$ and $\{\bar{\epsilon}\} = \{|\varepsilon_1|\ |\varepsilon_1|\ |\varepsilon_2|\ |\varepsilon_2|\ |\varepsilon_3|\ (\varepsilon_{31}^2 + \varepsilon_{23}^2)^{1/2}\}$

$$\{E_{RT}\} = \{E_0\}\left[1 + \{C_{rate1}\}\ln\left(\left\{\frac{\dot{\bar{\epsilon}}}{\dot{\bar{\epsilon}}_0}\right\}\right)\right] \tag{15}$$

where $\{E\} = \{E_a\ E_b\ E_c\ G_{ab}\ G_{bc}\ G_{ca}\}$, $\{\bar{\epsilon}\} = \{|\varepsilon_1|\ |\varepsilon_2|\ |\varepsilon_3|\ |\varepsilon_{12}|\ |\varepsilon_{23}|\ |\varepsilon_{31}|\}$ and $\{C_{rate1}\} = \{C_{rate2}\ C_{rate2}\ C_{rate4}\ C_{rate3}\ C_{rate3}\ C_{rate3}\}$.

Table 3. MAT_162 input parameters for Kevlar29/Epoxy.

Symbol	Property	Value
ρ	Density	1025 kg/m^3 (Scazzosi et al. 2018)
E_a	Elastic modulus 1	10.06 GPa (Scazzosi et al. 2018)
E_b	Elastic modulus 2	10.06 GPa (Scazzosi et al. 2018)
E_c	Elastic modulus 3	6 GPa (Bresciani et al. 2016)
ν_{ba}	Poisson's ratio 21	0.25 (Bresciani et al. 2016)
ν_{ca}	Poisson's ratio 31	0.33 (Bresciani et al. 2016)
ν_{cb}	Poisson's ratio 32	0.33 (Bresciani et al. 2016)
G_{ab}	Shear modulus 12	0.77 GPa (Bresciani et al. 2016)
G_{bc}	Shear modulus 23	5.43 GPa (Bresciani et al. 2016)
G_{ca}	Shear modulus 31	5.43 GPa (Bresciani et al. 2016)
S_{aT}	Tensile strength 1	405 MPa (Scazzosi et al. 2018)
S_{aC}	Compressive strength 1	185 MPa (Bresciani et al. 2016)
S_{bT}	Tensile strength 2	405 MPa (Scazzosi et al. 2018)
S_{bC}	Compressive strength 2	185 MPa (Bresciani et al. 2016)
S_{cT}	Through thickness tensile strength	34.5 MPa (Y. Q. Li, Li, and Gao 2015)
S_{FC}	Crush strength	1200 MPa (Y. Q. Li, Li, and Gao 2015)
S_{FS}	Fiber mode shear strength	1086 MPa (Y. Q. Li, Li, and Gao 2015)
S_{AB}	Matrix mode shear strength plane 12	77 MPa (Y. Q. Li, Li, and Gao 2015)
S_{BC}	Matrix mode shear strength plane 23	898 MPa (Y. Q. Li, Li, and Gao 2015)
S_{CA}	Matrix mode shear strength plane 31	898 MPa (Y. Q. Li, Li, and Gao 2015)
SFFC	Scale factor for residual compressive strength	0.3 (Y. Q. Li, Li, and Gao 2015)
ϕ	Coulomb's friction angle	10° (Y. Q. Li, Li, and Gao 2015)
E_LIMT	Element eroding axial strain	4.5 (Y. Q. Li, Li, and Gao 2015)
S	Scale factor for the delamination criterion	1.2 (Y. Q. Li, Li, and Gao 2015)
OMGMX	Limit damage parameter for the elastic modulus reduction	0.9975 (Y. Q. Li, Li, and Gao 2015)
ECRSH	Limit compressive relative volume for the element eroding	0.001 (Y. Q. Li, Li, and Gao 2015)
EEXPN	Limit tensile relative volume for the element eroding	5 (Y. Q. Li, Li, and Gao 2015)
AM1	Coefficient for the strain softening property	0.5 (Y. Q. Li, Li, and Gao 2015)
AM2	Coefficient for the strain softening property	0.5 (Y. Q. Li, Li, and Gao 2015)
AM3	Coefficient for the strain softening property	1 (Y. Q. Li, Li, and Gao 2015)
AM4	Coefficient for the strain softening property	20 (Y. Q. Li, Li, and Gao 2015)
C_{rate1}	Coefficient for the strain rate dependence	0.0257 (Y. Q. Li, Li, and Gao 2015)
C_{rate2}	Coefficient for the strain rate dependence	0.0246 (Y. Q. Li, Li, and Gao 2015)
C_{rate3}	Coefficient for the strain rate dependence	0.0246 (Y. Q. Li, Li, and Gao 2015)
C_{rate4}	Coefficient for the strain rate dependence	0 (Y. Q. Li, Li, and Gao 2015)

The element is eroded if one of the following three conditions is met:

- fiber tensile failure is predicted in both directions and the axial tensile strain is greater than E_LIMIT
- the compressive relative volume in a failed element is smaller than ECRSH
- the tensile relative volume in a failed element is greater than EEXPN

Also, the element is eroded if the maximum effective strain is greater than 100%. This additional erosion criterion is added, using the card MAT_ADD_EROSION, to remove overstrained elements.

The material input parameters for Kevlar29/Epoxy are reported in Table 3.

MAT162 is implemented for solid elements, therefore the panel is modeled as only one monolithic part, with a constant-stress solid element with reduced integration with viscous-type hourglass control. By using the meshing technique explained in (Material Science Corporation (MSC) & University of Delaware Center for Composite Materials (UD-CCM) 2017), the material model automatically detects delamination planes. Therefore, it is not necessary to model each layer as a separate part with a substantial reduction of contact interfaces and therefore of the computational cost of the simulation. It is preferred that each layer is represented by at least three elements trough the thickness so that delamination, once it has occurred, is assigned to one third of the layer. For this reason, the element dimensions are 1x1x0.148 mm where 0.148 is equal to one third to the average thickness of the layer. The numerical model implemented for MAT_162 is shown in Figure 1(b).

3. Discussion

The two numerical models with MAT_058 and MAT_162 are compared in terms of efficiency and accuracy of the results. In Figure 3 the ballistic curve, calculated fitting the Recht-Ipson model (Recht and Ipson 1963) with the data points obtained with the two numerical models is compared with the experimental results obtained in (Scazzosi, Manes, and Giglio 2019).

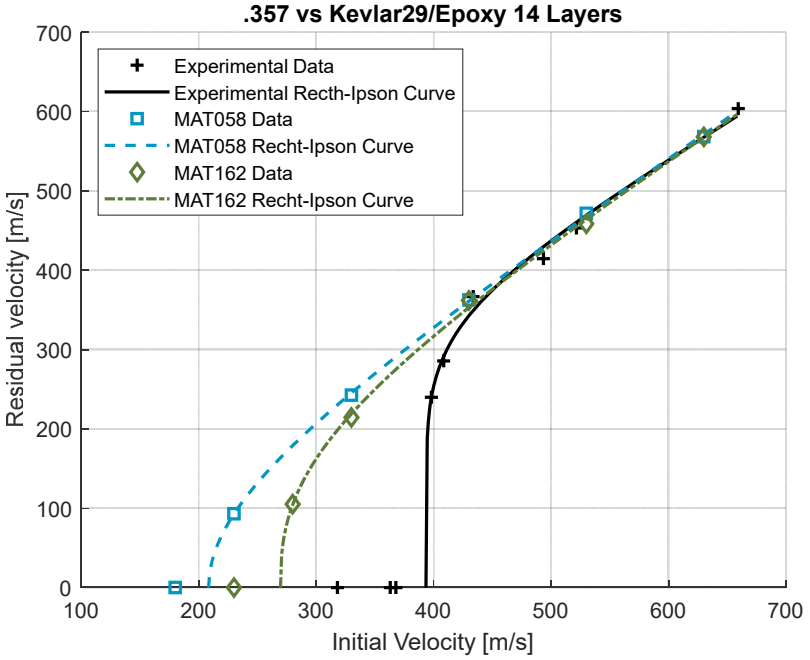

Fig. 3. Ballistic curves predicted with the numerical models and experimental result obtained in (Scazzosi, Manes, and Giglio 2019)

Both the two numerical model are extremely accurate for impact velocities higher than 430 m/s. Accuracy of the models is lower for impact velocities below 430 m/s approaching the ballistic limit velocity. In particular, MAT_162 is more accurate than MAT_058 since the error on the prediction of the ballistic limit is 32% for the former and 47% for the latter. The damage morphology of the two material models is compared in Figure 4: MAT_058 predicts more extended damage than MAT_162, the latter being more accurate in the reproduction of the experimentally observed damage morphology; furthermore, MAT_162 predicts a circular hole both in the front and the back face while MAT_058 predicts a less realistic hole of a rectangular shape. Even if the number of elements is 98992 for the numerical model of MAT_058 while it is 278192 for the numerical model of MAT_162, the former has a computational time of 2h46min while the latter has a computational time of 46min (time required to compute a simulation of 0.1 ms with 8 processors in message passing parallel mode). Therefore, the numerical model with MAT_162 is more efficient due to the absence of all the contact surfaces between each couple of adjacent layers since the panel is modelled as one part.

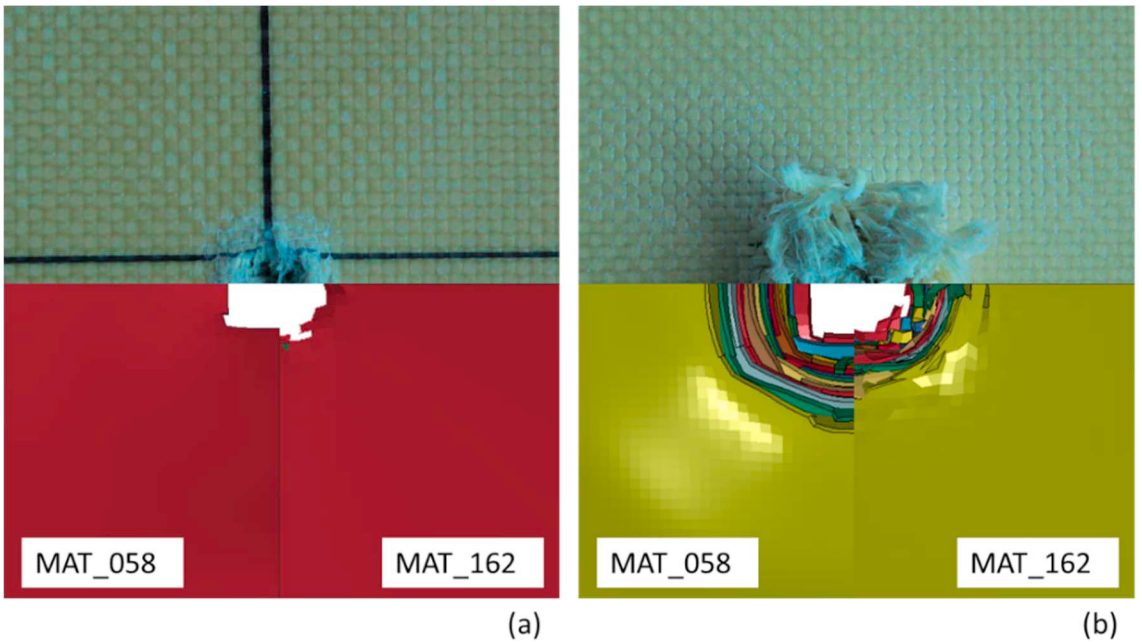

Fig. 4. Comparison between experimentally observed and predicted damage morphology for (a) front face and (b) back face.

According to Chu et al. tensile strength plays an important role in avoiding failure and therefore increases the ballistic performance (Chu, Ha-Minh, and Imad 2016). Therefore, relevant parameters that may affect the result of the simulation of high-velocity impact are the static tensile strength in the 11- and 22-direction. However, these parameters were obtained experimentally and cannot be modified arbitrarily. Regarding MAT_058, SLIMT1 and SLIMT2 are two parameters that may also affect the result. These values define the residual strength of the material after failure and therefore the energy absorbed by the element. Therefore, a parametric study was performed on the parameters SLIMT1 and SLIMT2 where their values were changed but, SLIMT1 was always considered to be equal to SLIMT2. The ballistic curves obtained with this parametric study are shown in Figure 5(a). By using a value of SLIMT1 = SLIMT2 = 0.05, which is lower than the baseline value of 0.1, the accuracy of the ballistic limit velocity is slightly reduced (reduction of the ballistic limit velocity of only 10% with respect to the baseline). This is to be expected since by lowering this value the energy absorbed by the element before it is eroded decreases. The

accuracy is still high for impact velocities above 430 m/s. By using a value of SLIMT1 = SLIMT2 = 0.2, which is higher than the baseline value of 0.1 and out of the recommended range (Livemore Software Technology Corporation (LSTC) 2017) ballistic limit velocity is increased by 30% with respect to the baseline value. This means that the accuracy of the predicted ballistic limit velocity is increased but the accuracy of the ballistic model for impact velocities above 430 m/s is reduced.

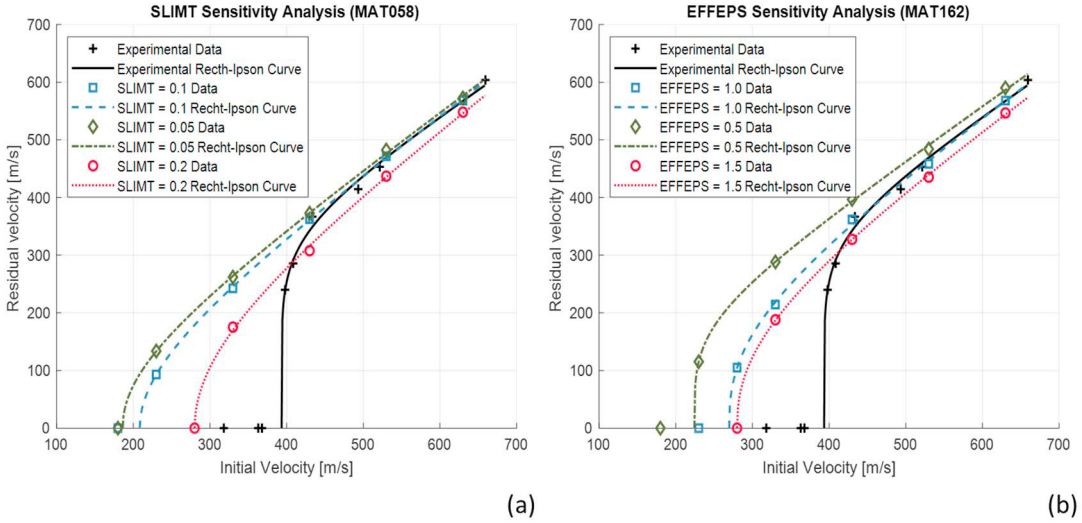

Fig. 5. Parametric study on (a) SMILT1 and SLIMT2 with MAT_058 and (b) C_{rate1} with MAT_162.

Regarding the numerical model implemented with Mat_162, the additional erosion criterion on maximum effective strain (EFFEPS) may affect the results also. According to (Barauskas and Abraitiene 2013), this value must be chosen so that it does not affect the failure criterion and that the model is not polluted by overstrained elements. As it can be seen in Figure 5 (b) the baseline value of EFFEPS = 1.0 leads to the most accurate estimation of the ballistic curve for impact velocities higher than 430 m/s. A value of EFFEPS = 0.5 seems to affect the failure criteria since the predicted ballistic limit velocity is lower. A value of EFFEPS = 1.5 leads to similar results to the baseline value, but the accuracy is slightly lower.

4. Conclusion

Two numerical models were developed to simulate high-velocity impact on fiber-reinforced composites using two different material model for the target. The first was Laminated Composite Fabrics (MAT_058) which is based on Matzenmiller, Lubliner and Taylor constitutive model for anisotropic damage in fiber-reinforced composites. The second was Composite MSC (in particular MAT_162) which may be used to model progressive failure of either unidirectional or woven fabrics composites. In particular, MAT_162 allows to model delamination without the necessity of physical interface between the layers and considers the effect of strain rate on the strength and moduli properties of the materials by means of a logarithmic function. MAT_162 showed more accuracy in the prediction of the ballistic limited velocity and lower computational time. Indeed, MAT_162 allowed to model delamination without the need of modelling each layer as a separate entity. This leads to a lower number of contact interfaces and therefore a lower computational cost. MAT_162 was also more accurate in the reproduction of the damage morphology. A parametric study showed that the parameters SLIMT1, SLIMT2 and EFFEPS affect the result of the numerical simulation.

References

Barauskas, Rimantas, and Ausra Abraitiene. 2013. "Multi-Resolution Finite Element Models for Simulation of the Ballistic Impact on Non-Crimped Composite Fabric Packages." *Composite Structures* 104 (October): 215–29. https://doi.org/10.1016/j.compstruct.2013.04.014.

Berk, Bulut, Ramazan Karakuzu, and Ahmet Kaan Toksoy. 2017. "An Experimental and Numerical Investigation on Ballistic Performance of Advanced Composites." *Journal of Composite Materials* 51 (25): 3467–80. https://doi.org/10.1177/0021998317691810.

Børvik, T., S. Dey, and A.H. Clausen. 2009. "Perforation Resistance of Five Different High-Strength Steel Plates Subjected to Small-Arms Projectiles." *International Journal of Impact Engineering* 36 (7): 948–64. https://doi.org/10.1016/j.ijimpeng.2008.12.003.

Bresciani, L.M., A. Manes, A. Ruggiero, G. Iannitti, and M. Giglio. 2016. "Experimental Tests and Numerical Modelling of Ballistic Impacts against Kevlar 29 Plain-Woven Fabrics with an Epoxy Matrix: Macro-Homogeneous and Meso-Heterogeneous Approaches." *Composites Part B: Engineering* 88 (March): 114–30. https://doi.org/10.1016/j.compositesb.2015.10.039.

Chu, Tuan-Long, Cuong Ha-Minh, and Abdellatif Imad. 2016. "A Numerical Investigation of the Influence of Yarn Mechanical and Physical Properties on the Ballistic Impact Behavior of a Kevlar KM2 ® Woven Fabric." *Composites Part B: Engineering* 95 (June): 144–54. https://doi.org/10.1016/j.compositesb.2016.03.018.

Deka, L. J., S. D. Bartus, and U. K. Vaidya. 2008. "Damage Evolution and Energy Absorption of E-Glass/Polypropylene Laminates Subjected to Ballistic Impact." *Journal of Materials Science* 43 (13): 4399–4410. https://doi.org/10.1007/s10853-008-2595-0.

Gama, Bazle A., and John W. Gillespie. 2011. "Finite Element Modeling of Impact, Damage Evolution and Penetration of Thick-Section Composites." *International Journal of Impact Engineering* 38 (4): 181–97. https://doi.org/10.1016/j.ijimpeng.2010.11.001.

Gilioli, A., A. Manes, M. Giglio, and T. Wierzbicki. 2015. "Predicting Ballistic Impact Failure of Aluminium 6061-T6 with the Rate-Independent Bao–Wierzbicki Fracture Model." *International Journal of Impact Engineering* 76 (February): 207–20. https://doi.org/10.1016/j.ijimpeng.2014.10.004.

Gower, H.L., D.S. Cronin, and A. Plumtree. 2008. "Ballistic Impact Response of Laminated Composite Panels." *International Journal of Impact Engineering* 35 (9): 1000–1008. https://doi.org/10.1016/j.ijimpeng.2007.07.007.

Jordan, Joseph B., Clay J. Naito, and Bazle Z. Haque. 2014. "Quasi-Static, Low-Velocity Impact and Ballistic Impact Behavior of Plain Weave E-Glass/Phenolic Composites." *Journal of Composite Materials* 48 (20): 2505–13. https://doi.org/10.1177/0021998313499952.

Kumar, Sunil, Durga Shankar Gupta, Inderdeep Singh, and Apurbba Sharma. 2010. "Behavior of Kevlar/Epoxy Composite Plates Under Ballistic Impact." *Journal of Reinforced Plastics and Composites* 29 (13): 2048–64. https://doi.org/10.1177/0731684409343727.

Li, Jintao, Chao Huang, Tian Ma, Xiancong Huang, Weiping Li, and Moubin Liu. 2019. "Numerical Investigation of Composite Laminate Subjected to Combined Loadings with Blast and Fragments." *Composite Structures* 214 (November 2018): 335–47. https://doi.org/10.1016/j.compstruct.2019.02.019.

Li, X.G., X.-L. Gao, and S. Kleiven. 2016. "Behind Helmet Blunt Trauma Induced by Ballistic Impact: A Computational Model." *International Journal of Impact Engineering* 91 (May): 56–67. https://doi.org/10.1016/j.ijimpeng.2015.12.010.

Li, Y. Q., X. G. Li, and X.-L. Gao. 2015. "Modeling of Advanced Combat Helmet Under Ballistic Impact." *Journal of Applied Mechanics* 82 (11): 111004. https://doi.org/10.1115/1.4031095.

Livemore Software Technology Corporation (LSTC). 2017. "LS-DYNA Keyword User's Manual - Volume II - Material Models."

Mallick, P. K. 2007. "Fiber-Reinforced Composites: Materials, Manufacturing, and Design."

Manes, A., L.M. Bresciani, and M. Giglio. 2014. "Ballistic Performance of Multi-Layered Fabric Composite Plates Impacted by Different 7.62mm Calibre Projectiles." *Procedia Engineering* 88: 208–15.

https://doi.org/10.1016/j.proeng.2014.11.146.
Material Science Corporation (MSC) & University of Delaware Center for Composite Materials (UD-CCM). 2017. "A Progressive Comosite Damage Model for Unidircetional and Woven Fabric Composites."
Matzenmiller, A, J Lubliner, and R.L. Taylor. 1995. "A Constitutive Model for Anisotropic Damage in Fiber-Composites." *Mechanics of Materials* 20 (2): 125–52. https://doi.org/10.1016/0167-6636(94)00053-0.
Nayak, N., A. Banerjee, and T.R. Panda. 2017. "Numerical Study on the Ballistic Impact Response of Aramid Fabric- Epoxy Laminated Composites by Armor Piercing Projectile." *Procedia Engineering* 173: 230–37. https://doi.org/10.1016/j.proeng.2016.12.002.
Nunes, Stephanie Gonçalves, Riccardo Scazzosi, Andrea Manes, Sandro Campos Amico, Wanderley Ferreira de Amorim Júnior, and Marco Giglio. 2019. "Influence of Projectile and Thickness on the Ballistic Behavior of Aramid Composites: Experimental and Numerical Study." *International Journal of Impact Engineering* 132 (October): 103307. https://doi.org/10.1016/j.ijimpeng.2019.05.021.
Recht, R. F., and T. W. Ipson. 1963. "Ballistic Perforation Dynamics." *Journal of Applied Mechanics* 30 (3): 384. https://doi.org/10.1115/1.3636566.
Scazzosi, R., A. Manes, and M. Giglio. 2019. "Analytical Model of High-Velocity Impact of a Deformable Projectile Against Textile-Based Composites." *Journal of Materials Engineering and Performance*, April. https://doi.org/10.1007/s11665-019-04026-x.
Scazzosi, R, A Manes, G Petrone, and M Giglio. 2018. "Two Different Modelling Approaches for Fabric Composites Subjected to Ballistic Impact." *IOP Conference Series: Materials Science and Engineering* 406: 012051. https://doi.org/10.1088/1757-899X/406/1/012051.
Schweizerhof, K., K. Weimar, Th. Munz, and Th. Rottner. 1998. "Crashworthiness Analysis with Enhanced Composite Material Models in LS-DYNA - Merits and Limits." In *LS-DYNA World Conference*. Detroit, Michigan, USA.
Tham, C.Y., V.B.C. Tan, and H.P. Lee. 2008. "Ballistic Impact of a KEVLAR® Helmet: Experiment and Simulations." *International Journal of Impact Engineering* 35 (5): 304–18. https://doi.org/10.1016/j.ijimpeng.2007.03.008.
Xiao, J.R., B.A. Gama, and J.W. Gillespie. 2007. "Progressive Damage and Delamination in Plain Weave S-2 Glass/SC-15 Composites under Quasi-Static Punch-Shear Loading." *Composite Structures* 78 (2): 182–96. https://doi.org/10.1016/j.compstruct.2005.09.001.
Zukas, Jonas A. 1990. *High Velocity Impact Dynamics*.